DOI: 10.1002/cbic.200900019

A Combined Solid-State NMR and MD Characterization of the Stability and Dynamics of the HET-s(218-289) Prion in its Amyloid Conformation

Adam Lange,* Zrinka Gattin, Hélène Van Melckebeke, Christian Wasmer, Alice Soragni, Wilfred F. van Gunsteren,* and Beat H. Meier*[a]

The three-dimensional structure of amyloid fibrils of the prion-forming part of the HET-s protein [HET-s(218–289)], as determined by solid-state NMR, contains rigid and remarkably well-ordered parts, as witnessed by the narrow solid-state NMR line widths for this system. On the other hand, high-resolution magic-angle-spinning (HRMAS) NMR results have shown that HET-s(218–289) amyloid fibrils contain highly flexible parts as well. Here, we further explore this unexpected behaviour using solid-state NMR and molecular dynamics (MD). The NMR data provide new information on order and dynamics in the rigid and flexible parts of HET-s(218–289), respectively. The MD study addresses whether or not small multimers, in an amyloid conformation, are stable on the 10 ns timescale of the MD run and provides insight into the dynamic parameters on the nanosecond timescale. The atom-positional, root-mean-squared fluctuations (RMSFs) and order parameters S^2 obtained are in agreement with the NMR data. A flexible loop and the N terminus exhibit dynamics on the ps–ns timescale, whereas the hydrophobic core of HET-s(218–289) is rigid. The high degree of order in the core region of HET-s(218–289) amyloids, as observed in the MD simulations, is in agreement with the narrow, solid-state, NMR lines. Finally, we employed MD to predict the behaviour of the salt-bridge network in HET-s(218–289), which cannot be obtained easily by experiment. Simulations at different temperatures indicated that the network is highly dynamic and that it contributes to the thermostability of the HET-s(218–289) amyloids.

Introduction

Prions are responsible for transmissible diseases where the agent is a conformationally altered protein of the host organism. Examples of prion diseases are scrapie in sheep,[1] bovine spongiform encephalopathy[2] (BSE) in cattle and new variant Creutzfeldt–Jakob disease[3] in man. In contrast to these disease-related cases, the HET-s prion protein produced by the filamentous fungus *Podospora anserina* is thought to be involved in a specific function. In its prion form it plays a role in the programmed-cell-death phenomenon termed "heterokaryon incompatibility",[4,5] which can prevent different forms of parasitism. The proteinase K-resistant core of the prion fibrils formed by the C-terminal residues 218–289 is unstructured in solution and forms infectious fibrils in vitro.[6] Earlier work showed that HET-s(218–289) fibrils consist of four β-strands forming two windings of a β-solenoid.[7] Recently, the structure of HET-s(218–289) has been determined[8] on the basis of NMR-derived intra- and intermolecular distance restraints.[9,10] The HET-s(218–289) prion exhibits a ^{13}C line width of 0.25–0.5 ppm rivalling those of microcrystalline preparations.[11] This suggests that the HET-s(218-289) fibrils are highly ordered. On the other hand, HRMAS experiments have shown that parts of HET-s(218–289) are flexible.[12] Similar observations have been made for amyloids formed by Tau,[13] α-Synuclein,[14] and the Y145Stop variant of the human prion protein.[15]

Recent advances in hardware and methodology[16] have allowed for molecular dynamics (MD) simulations of small fibrils consisting of several monomer units on the nanosecond timescale.[17–21] Herein, we have performed simulations of a HET-s(218–289) trimer in explicit solvent within a classical model (GROMOS force field parameter set 45A3).[22] The starting conformation is shown in Figure 1 A and B. One of the key features of amyloid fibrils is their structural stability. In this work, we used MD simulations as a tool to probe the stability of the solid-state NMR structure of HET-s(218–289) amyloids on a 10 ns timescale. Furthermore, we compared the conformational dynamics observed in the simulation with results from two complementary types of NMR experiments. In an $^{15}N,^{13}C_\alpha$ correlation experiment that is based on transfer mediated by dipolar couplings, only rigid parts of the amyloid contribute to the spectrum. In contrast, only flexible parts, in which dynamics lead to an efficient scaling of dipolar couplings, give rise to cross peaks in INEPT-based experiments.[23] The scaling of dipolar couplings with a coupling constant ω_D is described by an order parameter[24] S^2: The motionally averaged dipolar cou-

[a] *Dr. A. Lange, Z. Gattin, Dr. H. Van Melckebeke, C. Wasmer, A. Soragni, Prof. Dr. W. F. van Gunsteren, Prof. Dr. B. H. Meier*
Physical Chemistry, ETH Zürich
Wolfgang-Pauli-Strasse 10, 8093 Zürich (Switzerland)
Fax: (+41) 446-321-621
E-mail: adla@nmr.phys.chem.ethz.ch
wfvgn@igc.phys.chem.ethz.ch
beme@ethz.ch

Supporting information for this article is available on the WWW under http://dx.doi.org/10.1002/cbic.200900019.

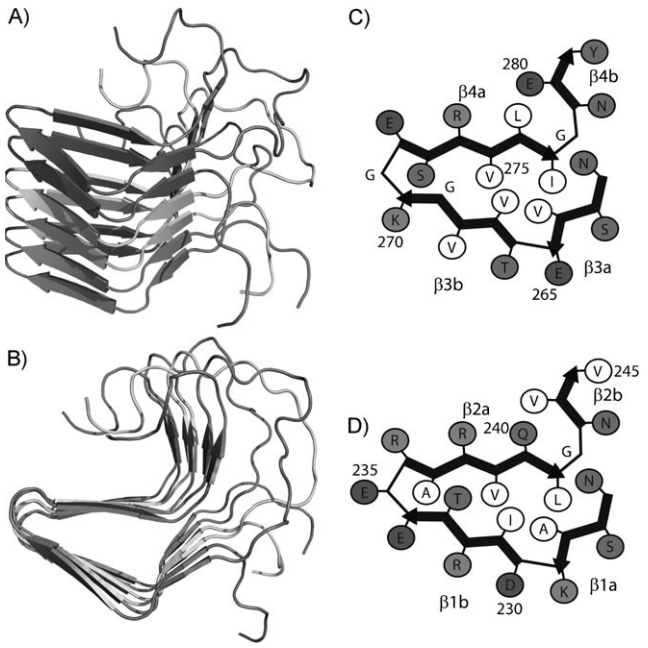

Figure 1. A) Side view of a HET-s(218–289) fibril. All MD calculations were performed on a HET-s(218–289) trimer. B) Top view. (C and D) Schematic representation of the two windings in each HET-s(218–289) molecule: The first winding [N226–V245, displayed in D)] of the β solenoid is located beneath the second one [N262–Y281, displayed in C)].

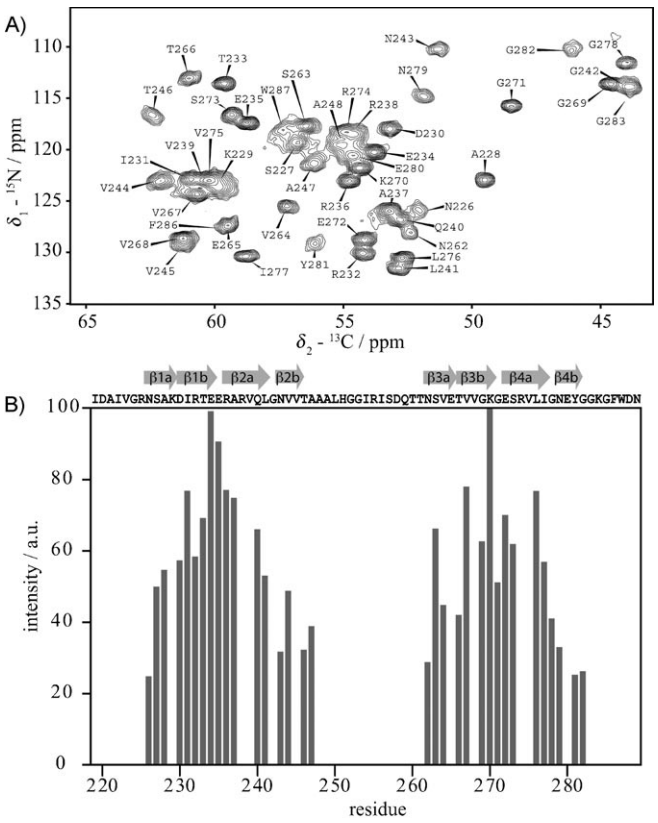

Figure 2. A) $^{15}N,^{13}C_\alpha$ correlation spectrum of HET-s(218–289) amyloid fibrils. The spectrum was recorded on a 850 MHz wide-bore spectrometer at a probe temperature of −10 °C (corresponding sample temperature 5–10 °C) and at 19 kHz magic-angle spinning. B) The cross-peak intensity in the $^{15}N,^{13}C_\alpha$ correlation spectrum is plotted as a function of the residue number.

pling ω_D^{eff} is given by $(\omega_D^{eff})^2 = S^2\omega_D^2$. The order parameter S^2 can also be calculated from MD simulations and, therefore, the simulations can provide an atomic-level understanding of the large dynamical heterogeneity observed in the HET-s(218–289) fibrils; while the core is very rigid, the loop of roughly a dozen residues connecting the rigid β sheets β2b and β3a (see Figures 1 and 4B) are highly flexible with an almost isotropic motion on the NMR timescale.

A fascinating feature of HET-s(218–289) amyloids is the abundant network of surface salt bridges. A full experimental characterization is difficult, but our MD simulations at different temperatures provide an atomic-resolution picture of the dynamic nature of the network and its role in fibril stability.

Results and Discussion

Figure 2A shows a $^{15}N,^{13}C_\alpha$ correlation spectrum of HET-s(218–289) amyloid fibrils recorded on a 850 MHz spectrometer. The experiment is based on dipole-mediated polarization transfer, and therefore, only residues with high-order parameters[25,26] S^2 (on the NMR timescale of ms) give rise to signals. Typical observed line widths were 0.9 ppm and 0.5 ppm for ^{15}N and ^{13}C, respectively. Virtually all residues that are part of the triangular core region (N226–L241 and N262–I277) of HET-s(218–289) contribute to the spectrum. A detailed scheme of the side-chain arrangement in the core region is given in Figure 1C and D for the two pseudo-repeats that form the two layers of the β solenoid. The signal intensities for the resolved cross peaks were extracted from the spectrum and are plotted in Figure 2B. The most intense resonances were observed for residues E234 and K270, which are on top of each other in the amyloid structure (Figure 1) and located at the ends of β-strands β1b and β3b, respectively. For the numbering of the β-strands see Figure 1C and D. In general, high intensities were observed for all residues that are located in β-strands with the exception of the residues in β-strands β2b and β4b, which are not part of the triangular core of the fibrils. These residues exhibited smaller intensities especially at the ends that point away from the hydrophobic core. No signals were observed for residues in the N and C termini (except a rather broad cross peak for W287) and the loop that connects the two layers; this indicates that they are either dynamically or statically disordered.

Figure 3 shows results from a series of INEPT-based ^{13}C-detected $^{1}H,^{13}C$ HETCOR experiments. In this type of experiments only relatively flexible residues with low-order parameters S^2 values give rise to signals. The observed line widths for ^{1}H and ^{13}C were typically 0.15 ppm and 0.5 ppm, respectively. The ^{13}C line width was probably dominated by unresolved ^{13}C–^{13}C couplings. Using a combination of $^{1}H,^{13}C$, $^{1}H,(^{13}C),^{13}C$ and $(^{1}H),^{13}C,^{13}C$ correlation spectra, we could assign the observed signals to specific amino acid types. We identified the following spin systems: 1×Ala, 1×Glu, ≥ 3×His, 1×Lys, 1×Leu, 1×Met, 1×Gln, 1×Arg, 1×Ser, 2×Asp, 2×Gly, 2×Ile, 2×Thr and 2×Val. The corresponding chemical shift assignments are listed

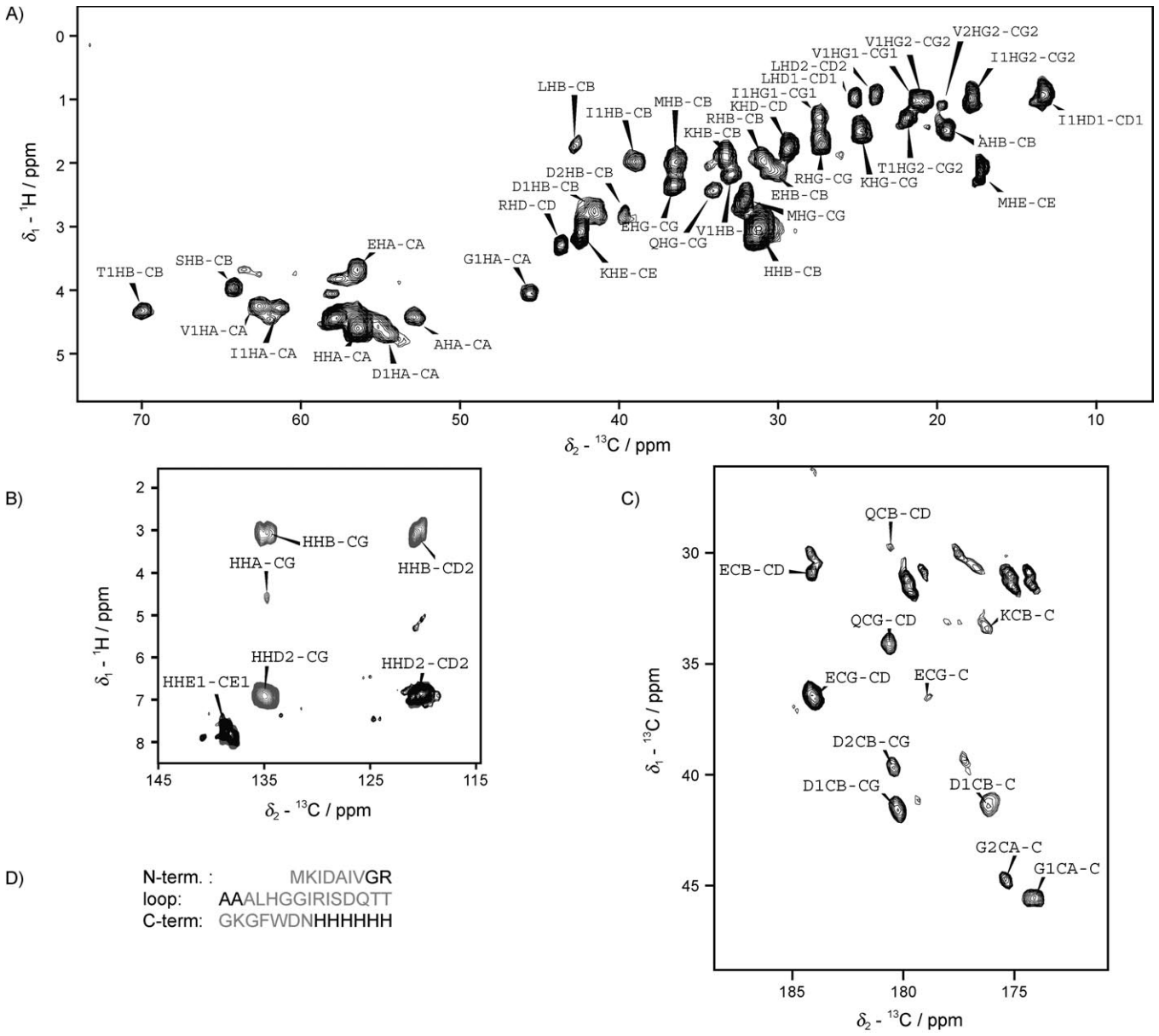

Figure 3. A)–C) NMR spectra that were recorded utilizing an initial $^{1}H,^{13}C$ INEPT transfer step. Therefore, only mobile residues that have long enough transverse dephasing times T_2 give rise to cross peaks. A) Aliphatic region of a $^{1}H,^{13}C$ correlation spectrum. B) A $^{1}H,(^{13}C),^{13}C$ spectrum (in grey) overlaid with the $^{1}H,^{13}C$ spectrum (in black). The aromatic region of the spectra is shown. C) C′-C_α correlations in a $(^{1}H),^{13}C,^{13}C$ spectrum. The homonuclear ^{13}C polarization transfer in B) and C) was achieved via $P9_3^1$ TOBSY (mixing time: 6 ms). D) Tentative assignment of the observed residues to segments (in grey) in the flexible loop and the N and C termini.

in Table S1 in the Supporting Information. The assigned $^{13}C_\alpha$ and $^{13}C_\beta$ chemical shifts agree well with random-coil values from the Biological Magnetic Resonance Data Bank. This shows that the flexible parts are indeed unfolded. For His, one can identify at least three overlapping signal sets, which most probably represent the highly flexible C-terminal His-tag.

Notably, not all amino acid types that are present in the HET-s(218–289) sequence were found in the INEPT-spectra; Asn, Phe, Trp and Tyr were missing. Thus, the possibility that the assigned resonances belong to residual monomers in the sample can be excluded. The INEPT-based data is in full agreement with previous HRMAS studies; this also excluded the possibility of monomers on the basis of pulsed-field gradient methods.[12] We tentatively assigned the observed spin systems to the N and C termini and the flexible loop that connects the two pseudo repeats. The result is shown in Figure 3D. The observed amino acids correspond well with the sequence of the N terminus and the loop. In contrast, the C terminus did not give rise to cross peaks, as indicated by missing Phe, Trp and Asn resonances. Only the C-terminal His-tag was visible. The observed Glu resonance is difficult to explain. It possibly corresponds to E280 in a small population of the sample in which β-strand β4b is flexibly disordered. This would be in agreement with the low intensity $^{15}N,^{13}C_\alpha$ cross peak of E280 (see Fig-

ure 2). In line with this observation, the low-intensity second Val set could be attributed to a population of V245.

While experimentally measured NMR parameters report on ensemble properties, MD simulations are indicative of the properties of individual molecules. Combining the techniques can thus be useful in obtaining a more complete picture of the biomolecular system of interest. Herein, we performed atomistic MD simulations of HET-s(218–289) trimers in explicit water at two different temperatures ($T = 298$ K and $T = 323$ K) for 10 ns. Figure 4A shows the atom-positional root-mean-square deviations (RMSDs) from the energy-minimized and equilibrated HET-s(218–289) trimer conformation. The C_α atoms of residues N226–V245 and N262–Y281 of the middle molecule only (black line: 298 K; red line: 323 K) and of all three molecules (green line: 298 K; blue line: 323 K), respectively, were considered. In both cases and at both temperatures, the RMSDs reached a plateau well below 0.2 nm within the first 4 ns and stayed stable until the end of the simulations. This demonstrates that the simulated trimer is stable and does not dissociate on the investigated timescale. An MD conformational ensemble of the middle molecule at 298 K is depicted in Figure 4 (20 structures, sampled every 0.5 ns, fitting to the C_α atoms of residues N226–V245 and N262–Y281 of the middle molecule). The backbone of the triangular hydrophobic core exhibits a remarkable stability. Also the side chains that point into the core appear rather rigid, whereas the side chains on the outside are more mobile. Several NMR distance restraints place the hydrophobic side chain of W287 in the corner formed by β-strands β2a and β2b (and correspondingly β4a and β4b). The MD conformational ensemble indicates that the side chain of W287 stays in the same position (labelled in Figure 4D with an asterisk) although the C terminus in general exhibits more disorder. Also, the loop (residues A247–T261) and the N terminus appear disordered in the MD ensemble.

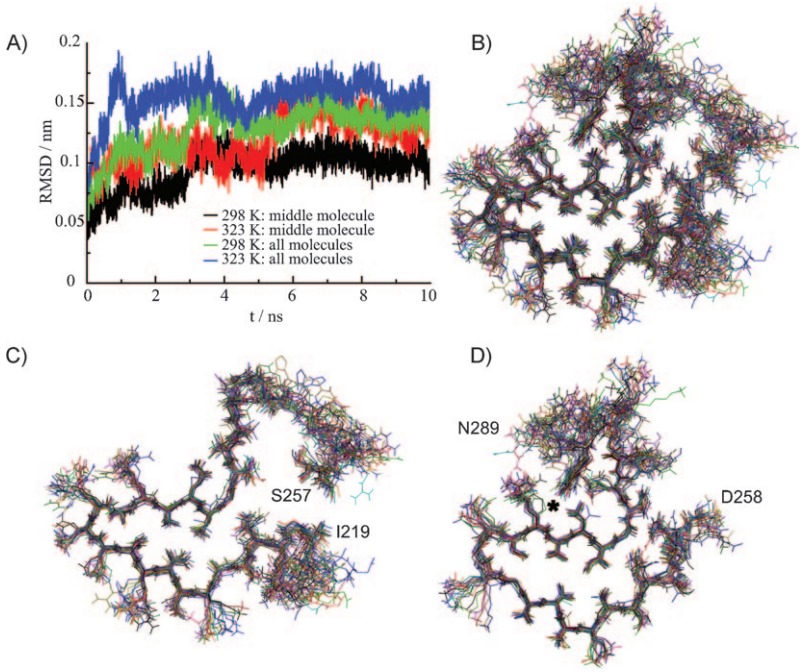

Figure 4. A) Atom-positional RMSD of MD trajectory structures from the energy-minimized and equilibrated HET-s trimer conformation. C_α atoms of residues N226–V245 and N262–Y281 of the middle molecule only (black line: 298 K; red line: 323 K) and of all three molecules (green line: 298 K; blue line: 323 K), respectively, were considered. (B, C and D) MD conformational ensemble of the middle molecule at 298 K (20 structures, sampled every 0.5 ns, fitting to C_α atoms of residues N226–V245 and N262–Y281 of the middle molecule). Residues I219–N289 are shown in B). In C), residues I219–S257 are shown, which comprise the N terminus, the first winding and the first part of the loop. Residues D258–N289 are shown in D) and include the second part of the loop, the second winding and the C terminus. The side chain of W287 is labelled with an asterisk.

To assess the dynamics quantitatively we calculated atom-positional root-mean-squared fluctuations (RMSFs) of the C_α atoms and NH order parameters S^2 from the MD simulations at the two temperatures. The results are shown in Figure 5. To remove the effects of overall tumbling, a fit to the C_α atoms of residues N226–V245 and N262–Y281 of the middle molecule preceded the calculation of S^2 (reference structure: after 5 ns of MD simulation). This is mandatory if the data are to be compared with NMR data recorded on fibrils comprising virtually thousands of stacked molecules. Only the second half of the trajectories was considered in the analyses since it might require several ns for the flexible loop to find an energetically favourable conformation. Order parameters were determined from Equation (1)

$$S^2 = {}^1\!/_2\left[3\sum_{\alpha=1}^{3}\sum_{\beta=1}^{3}\langle\mu_\alpha\mu_\beta\rangle^2 - 1\right] \quad (1)$$

where μ_α ($\alpha = 1, 2, 3$) are the x, y and z components of the normalized interatomic vector in the fibril-fixed axis system. This equation, derived in ref. [24] has favourable properties for the numerical evaluation of order parameters.[27,28] The averages involved 10000 frames sampled every 0.5 ps from 5 to 10 ns of MD simulation.

For residues in the β-strand conformation, we found very small RMSF values around 0.05 nm and order parameters S^2 of 0.8–0.9 (see Figure 5). In contrast, the loop connecting the two pseudorepeats and the N and C termini are characterized by larger RMSF values, above 0.1 nm, and smaller order parameters S^2 below 0.6. The smallest NH order parameters for residues in the loop were found for residues G252 and G253 (both 0.23). At the higher temperature, slightly larger RMSFs and slightly smaller order parameters were found for residues in the β-strand conformation and the N terminus. In contrast, smaller RMSFs and larger order parameters were observed for the loop and the C terminus. Since flexible segments could exhibit mobility on timescales that are not accessible by the 10 ns simulation, the calculated RMSFs and order parameters represent the lower and upper limits, respectively.

The calculated order parameters for W287 and F286, both in the C-terminal tail, which appear in the CP spectra and not in the INEPT spectra, were indeed higher and the RMSFs were smaller (see Figure 5) than for the residues in the long loop, in

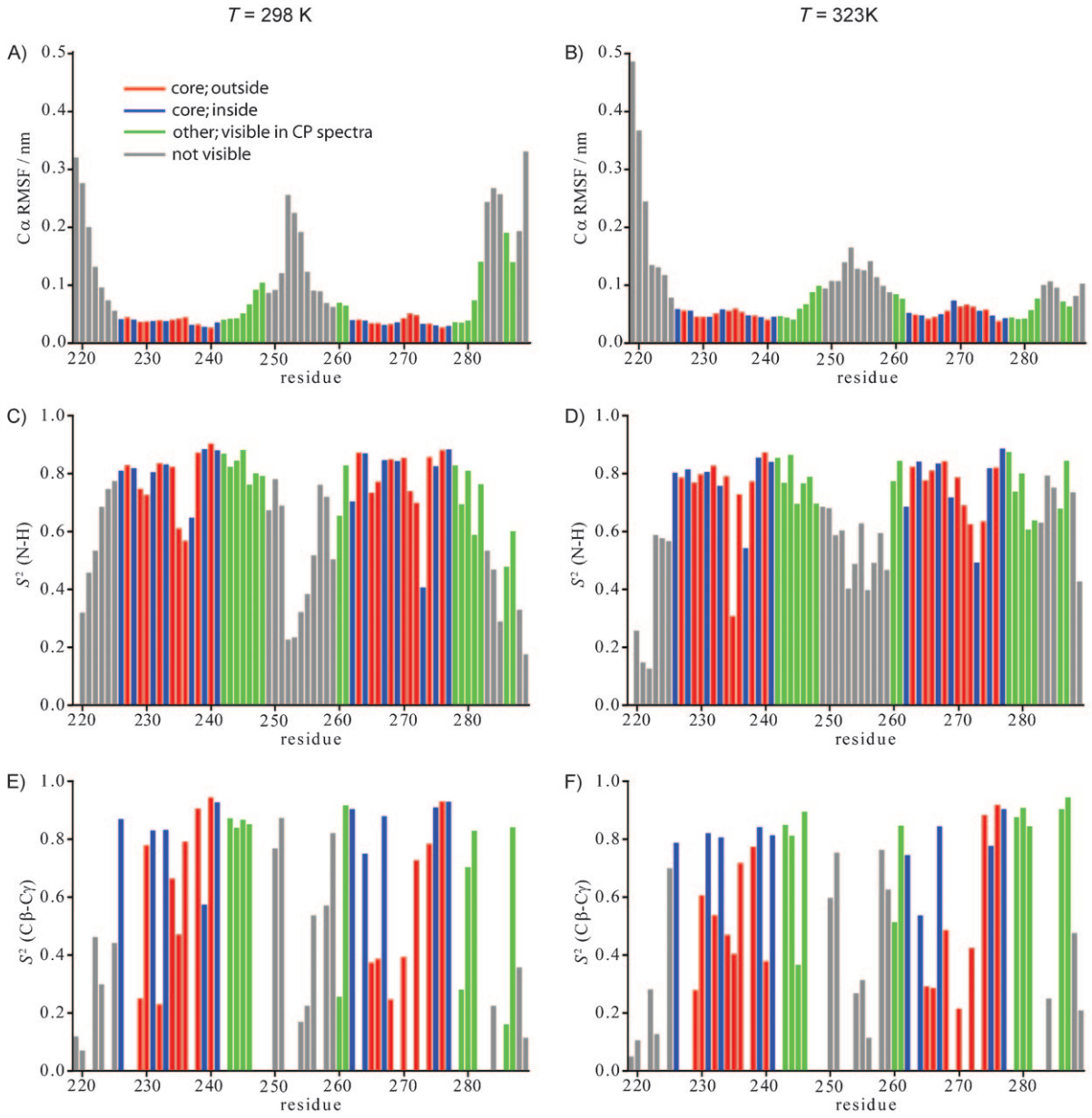

Figure 5. A) and B) Atom-positional RMSFs of C_α atoms of the middle molecule. Only the second halves of the trajectories (that is, 5–10 ns) are included in the analysis. Before the RMSF calculation a fit to C_α atoms of residues N226–V245 and N262–Y281 of the middle molecule was performed. Blue bars refer to residues that point into the hydrophobic core, residues in red point outwards. Residues in green are not part of the triangular core region but give rise to cross peaks in experiments based on cross polarization and are therefore considered rigid. The remaining residues are shown in grey. C)–F) Order parameters S^2 for the middle molecule. To remove the effects of overall tumbling a fit to C_α atoms of residues N226–V245 and N262–Y281 of the middle molecule preceded the calculation of S^2 (reference structure: at 5 ns MD run). Only the second halves of the trajectories were considered. C) and D) NH order parameters. E) and F) C_β-C_γ(2) order parameters. A), C) and E) $T = 298$ K; B), D) and F) $T = 323$ K.

agreement with the experimental findings. This behaviour is also reflected in Figure 4D, where this part seemed quite ordered. Note that the side chain of W287 is marked with an asterisk.

Additionally, we calculated order parameters for isoleucine side chains, which can be found in the N terminus, the loop and the hydrophobic core. The results are shown in Table 1. For the C_β-$C_{\gamma 1}$, S^2 at $T = 323$ K, we determined values between 0.05 for the N-terminal I219 and 0.8–0.9 for I231 and I277, which are found in the hydrophobic core. The corresponding

Table 1. Isoleucine side chain order parameters S^2 at $T = 298/323$ K.

Residue	C_α–C_β	C_β–$C_{\gamma 1}$	$C_{\gamma 1}$–C_δ
I219	0.58/0.17	0.16/0.05	0.24/0.03
I222	0.80/0.27	0.44/0.39	0.31/0.16
I231	0.95/0.94	0.84/0.83	0.32/0.11
I254	0.40/0.73	0.11/0.24	0.10/0.26
I256	0.86/0.43	0.47/0.12	0.48/0.10
I277	0.97/0.96	0.94/0.92	0.78/0.51

values for the loop residues I254 and I256 are 0.24 and 0.12, respectively. This fits well with the experimental observations. In general, the agreement is better at the higher temperature, possibly due to better sampling of the conformational space. On the other hand, the calculated $C_{\gamma 1}$-C_{δ} order parameters seemed to be slightly too small since at least in the case of I231 and I277, $C_{\gamma 1}$-C_{δ} cross peaks could be observed in dipolar-mediated correlation experiments (see for example, the spectrum shown in Figure 2 of ref. [4]). We also calculated S^2 for C_{β}-C_{γ} for all residues but Ala, Gly and Ser. The results are shown in Figure 5E and F. In general, side chains that point into the hydrophobic core (depicted in blue) are characterized by large S^2 values around 0.8.

Next, we analysed the salt-bridge network in HET-s(218–289). According to the NMR structure, the core of HET-s(218–289) amyloids contains six positively and six negatively charged side chains that are all solvent exposed (Figure 1C and D). There are three short-distance pairs of counter charges that could potentially form salt bridges: K229–E265, E234–K270 and R236–E272. Several distance restraints that were derived from NMR experiments[8] support the existence of these salt bridges. Because the stacking is parallel, the charge compensation could be both intra- and intermolecular in nature. Figure 6 shows an overview of the observed salt bridges in the core region of HET-s(218–289). The network appeared very dynamic on the ps–ns timescale. Intra- as well as intermolecular K229–E265 salt bridges, for example, were occupied during 34% and 24%, respectively, of the simulation at $T = 298$ K (36% and 25%, respectively, at 323 K; see also Figure 6C). The dynamic nature of the salt-bridge network is not surprising considering the relevant enthalpic and entropic contributions to the free energy of protein folding. The Coulomb interaction is not sensitive to dynamics as long as distances remain approximately the same (r^{-1} distance dependence), while a dynamic salt-bridge network is entropically favoured with respect to a static one. Indeed, the average salt bridge occupancy slightly increases with temperature (26 vs. 24%). This view is corroborated by an analysis of the nonbonded interaction energies between the molecules in the trimer and water. The intermolecular Coulomb interaction for the middle molecule of the trimer becomes more negative with a temperature increase from 298 to 323 K [from −2209(202) to −2484(223) kJ mol^{-1}], and the corresponding interaction with water becomes weaker [from −8387(438) to −8278(447) kJ mol^{-1}]. The values in parentheses refer to the RMSFs.

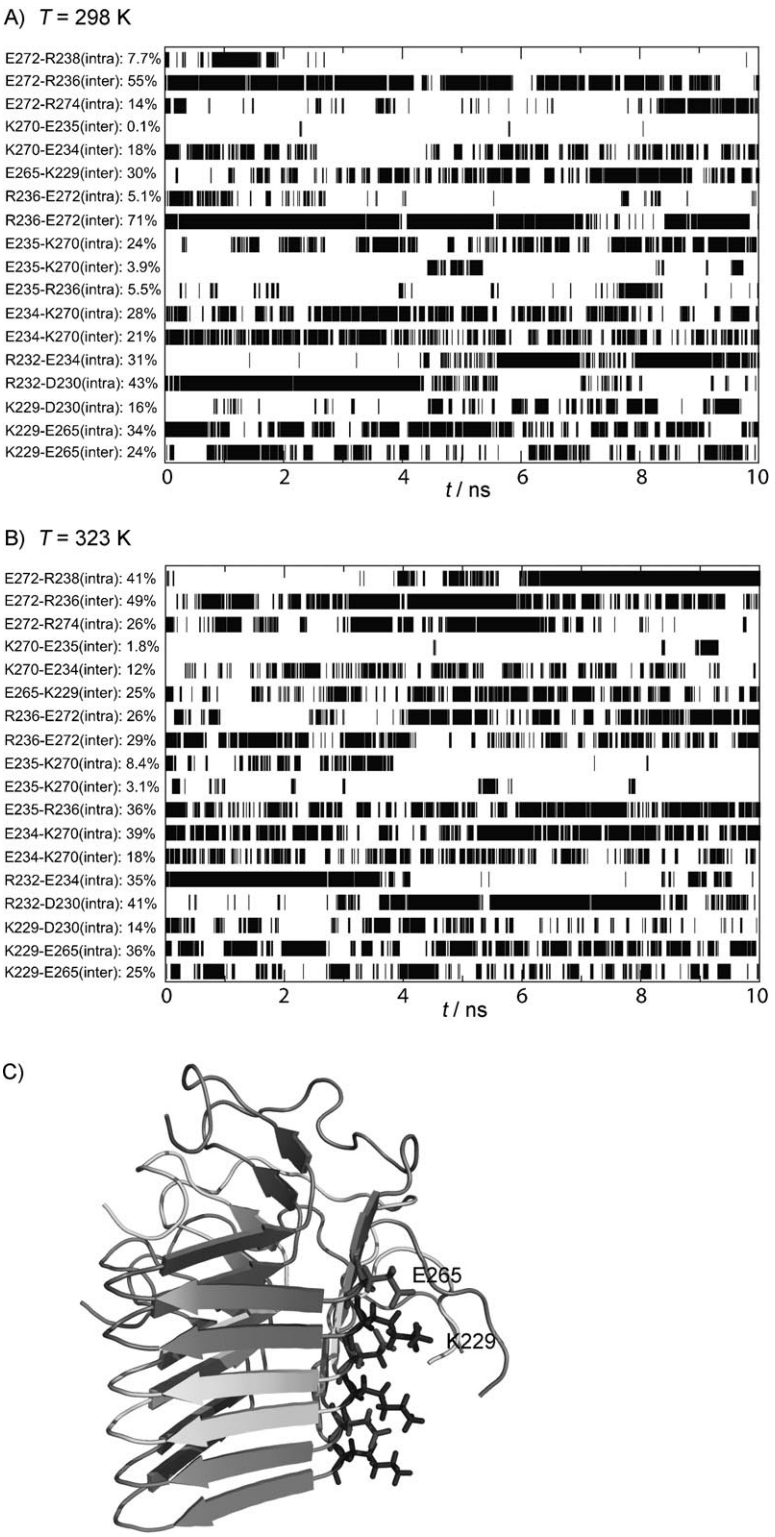

Figure 6. Analysis of the dynamic salt-bridge network at A) $T = 298$ K and B) $T = 323$ K. Distances between Lys N_{ζ} and Arg C_{ζ} atoms on the one hand and Asp C_{γ} and Glu C_{δ} atoms on the other hand were considered. The cutoff for salt-bridge interactions involving Arg and Lys was set to 0.6 and 0.5 nm, respectively. The residue that is listed first in the Figure legend is from the middle molecule. The partner can be either from the middle molecule as well (i.e., intramolecular) or from the first or third molecule (i.e., intermolecular). The average occupancy of the salt bridges is included in the legend. Vertical bars in the plot indicate the presence of the salt bridge at the given time point. C) Cartoon representation of the simulated HET-s(218–289) trimer. Residues E265 and K229 are shown in a stick representation.

Conclusions

The HET-s(218–289) prion in its amyloid conformation represents the only amyloid for which a high-resolution structure is available. Herein, we discuss new solid-state NMR data that report on order and disorder and explain them in terms of both the molecular structure and MD simulations of short fibril fragments in explicit water. The observed intensity variations in the two-dimensional $^{15}N,^{13}C_\alpha$ correlation spectrum correlate well with the NMR structure. An additional set of signals in experiments based on INEPT transfer could be attributed to the N terminus and the loop that connects the two pseudo repeats of HET-s(218–289). Narrow lines were observed in both types of experiments, albeit for different reasons. In the $^{15}N,^{13}C_\alpha$ spectrum, only parts of the protein that are both well-ordered and inflexible gave rise to sharp cross peaks. In the INEPT-based experiment, the dynamics of the observed flexible parts resulted in an averaging of isotropic chemical shifts, and broadening mechanisms, such as residual heteronuclear dipolar couplings, were diminished.

The simulated HET-s(218–289) trimer is stable on a 10 ns timescale. Since the simulated system is small in comparison to real HET-s(218–289) amyloids, which comprise virtually thousands of stacked molecules, this indicates that the observed fold is indeed remarkably stable. The MD ensemble of Figure 4B is, despite the different timescales involved, strikingly similar to the NMR bundle of the 20 lowest-energy structures (Figure 2C of ref. [8]) and features a well-defined core region. The observed dynamics, as reflected in RMSFs and NH order parameters, correlate well with the NMR data; a flexible loop and the N terminus exhibit dynamics on the picosecond–nanosecond timescale, whereas the hydrophobic core of HET-s(218–289) is rigid. Since scaling of dipolar couplings also takes place on a slower timescale (up to μs–ms), motion that is not adequately sampled in a 10 ns simulation will lead to a deviation between NMR data and results from MD simulations.[27] Especially disordered protein segments might require significantly longer to sample their conformational space. In contrast, the simulation timescale provides very well for the study of dynamics in the β-strand parts. In general, the calculated order parameters represent upper limits. A future direction of our work could be a direct comparison between NMR and MD order parameters. For this purpose, we would perform MD simulations on a longer timescale. Solid-state NMR order parameters would be measured similarly to the work by the groups of McDermott and Huster.[25,30]

Of particular interest in this work was the nature of the salt-bridge network in HET-s(218–289). The MD simulation showed that the network was highly dynamic on a ps–ns timescale. A comparison of the results obtained at $T = 298$ and 323 K indicated that HET-s(218–289) does not unfold over this range. Instead, electrostatic interactions are even slightly increased, a behaviour that is reminiscent of thermophile proteins.[31] A comparison of high-resolution structures of homologous proteins in mesophilic and thermophilic organisms has revealed several potentially stabilizing factors, such as rigidity, improved packing of side chains in the hydrophobic core, increased hydrogen bonding and, most strikingly, an increased number of salt-bridge networks.[29,32] Interestingly, these factors can also be found in HET-s amyloids, although the fungus *Podospora anserina* is not a thermophile organism.

Experimental Section

NMR spectroscopy: Uniformly [$^{13}C,^{15}N$] labelled HET-s(218–289) was recombinantly expressed in *E. coli*, purified and fibrillized at pH 7.5 as previously described.[33] Subsequently, the fibrils were washed 4–5 times in deionized water and centrifuged into magic-angle-spinning (MAS) rotors. To ensure a constant hydration level, the MAS rotor tips were glued to the rotors, and proper sealing was controlled by weighing the rotors before and after NMR measurements. The NMR samples contained approximately 70 weight percent water.

Two-dimensional NMR experiments were conducted on 14.1 and 20 T (corresponding ^1H resonance frequencies of 600 MHz and 850 MHz, respectively) wide-bore instruments (Bruker Biospin, Germany) equipped with 4 mm (600 MHz) and 3.2 mm (850 MHz) triple resonance probes. The MAS frequency was set to 10 kHz (600 MHz) and 19 kHz (850 MHz), respectively.

A $^{15}N,^{13}C_\alpha$ experiment[34] (total acquisition time: 18 h) was carried out at a sample temperature of 5–10 °C on the 20 T instrument. Proton-decoupling using the sequence SPINAL64[35] with an radio frequency amplitude of 100 kHz was applied during evolution and detection periods. Contact times were set to $t_{HN} = 1$ ms and $t_{NC} = 3$ ms for H→N and N→C transfer. Radio frequency fields of ~50 kHz on ^{15}N and ~70 kHz on ^1H with a linear ramp on ^1H were employed for the $^1H,^{15}N$ cross polarization. For the second step, radio frequency fields of ~50 kHz on ^{15}N and ~30 kHz on ^{13}C with a linear ramp on ^{13}C were used. Maximum t_1 and t_2 times were 19.2 ms (768 points) and 22.2 ms (3072 points), respectively.

INEPT-based experiments[36,37] were performed similarly as described by Andronesi et al.[23] $^1H,^{13}C$, $^1H,(^{13}C),^{13}C$ and $(^1H),^{13}C,^{13}C$ spectra were recorded at a sample temperature of 35–40 °C on the 600 MHz spectrometer. During ^{13}C evolution and detection periods, SPINAL64 decoupling with an radio frequency amplitude of 55 kHz was applied. In the middle of ^1H evolution periods, a ^{13}C −180° pulse was used to refocus the $^1H,^{13}C$ J interaction. For the heteronuclear polarization transfer, a refocused INEPT block with delays of $^1/_4J$, $^1/_4J$, $^1/_6J$, $^1/_6J$ with $J = 200$ Hz was employed. A $^1H,^{13}C$ spectrum was recorded in 27 h with maximum t_1 and t_2 times of 14.9 ms (372 points) and 20.5 ms (2048 points), respectively. For the homonuclear $^{13}C,^{13}C$ transfer in the $^1H,(^{13}C),^{13}C$ experiment (total acquisition time: 3 h; 128 and 2048 points in t_1 and t_2, respectively) and the $(^1H),^{13}C,^{13}C$ experiment (total acquisition time: 15 h; 824 and 2048 points in t_1 and t_2, respectively), a $P9^1_3$ TOBSY[38] sequence with a mixing time of 6 ms (corresponding to 20 full cycles) was applied.

All spectra were processed by using QSINE window functions in F1 and F2 and analysed by using SPARKY version 3.110 (T. D. Goddard and D. G. Kneller, University of California–San Francisco). The ^{13}C chemical shift scale was calibrated using adamantane as an external reference (upfield ^{13}C resonance: 31.47 ppm), which is consistent with DSS (internal). ^1H shifts were indirectly calibrated using a ^{13}C to ^1H ratio of $\Xi = 0.251449530$.[39]

Molecular dynamics simulations: Steepest-descent energy minimizations and MD simulations at constant temperature and pressure were carried out using the GROMOS05 biomolecular simula-

tion package[40] with the GROMOS force-field parameter set 45A3.[22]

An initial configuration of the HET-s(218–289) trimer was adapted from the solid-state NMR structure (PDB ID: 2RNM). The primary sequence used in the simulations was "NH_3^+-IDAIVGRNSAKDIRT-EERARVQLGNVVTAAALHGGIRISDQTTNSVETVVGKGESRVLIGNEYGGK-GFWDN-COO^-". Note that the six amino acid C-terminal His-tag and the first two residues of the expressed HET-s(218–289) construct (M217 and K218) were not considered; that is, the first simulated residue was I219. Since the NMR experiments were performed at neutral pH in a salt-free medium, all K, R, D and E residues were simulated in their charged state. H251 was assumed to be uncharged and protonated at $N_{\delta 1}$. This system is electrically neutral, and no further ions had to be considered. In a first round of energy minimization in vacuum, all side chains were allowed to move freely while the backbone atoms were position-restrained with a force constant of 2.5×10^4 kJ mol^{-1} nm^{-2}. The minimization terminated when the energy change per step became <0.1 kJ mol^{-1}. Next, the HET-s(218–289) trimer was solvated in 20559 pre-equilibrated water molecules, modelled according to SPC[41] water. The minimum distance from any atom of the peptide to the walls of the cubic box exceeded 1.6 nm. In a second round of energy minimization, the solute atoms were restrained and the solvent could relax. Finally, an energy minimization without any restraints was performed to remove residual strain.

Initial velocities for the MD simulations were taken from a Maxwell–Boltzmann distribution at 100 K. The temperature was then stepwise (five steps of 50 ps) increased to 298 K (simulation 1) and 323 K (simulation 2). Simultaneously, the restraints on the backbone atom positions were gradually loosened (the force constant during the first step: 2.5×10^4 kJ mol^{-1} nm^{-2}). In the last 50 ps, the pressure was kept constant at 1 atm. Solvent and solute were weakly coupled to separate temperature baths[42] with a relaxation time of 0.1 ps. Similarly, the pressure was coupled to a pressure bath[42] with a relaxation time of 0.5 ps and an isothermal compressibility of 0.4575×10^{-3} (kJ mol^{-1} nm^{-3})$^{-1}$. The SHAKE algorithm[43] was applied to constrain all bond lengths with a relative geometric tolerance of 10^{-4}, and a leap-frog integration time step of 2 fs was used. Nonbonded interactions were truncated at a distance of 1.4 nm and recalculated every time step in the range 0.0–0.8 nm and every five time steps in the range 0.8–1.4 nm using a twin-range cutoff scheme. Outside of 1.4 nm, a reaction field (relative dielectric permittivity: 61) approximated the electrostatic interactions.[44]

MD simulations were performed for 10 ns at both temperatures, and molecular configurations were extracted every 0.5 ps for further analysis.

Acknowledgements

We thank Dr. Paul Schanda and Dr. Sven Saupe for scientific discussions. Financial support by the ETH Zürich through the TH-grant system and by the National Center of Competence in Research (NCCR) Structural Biology of the Swiss National Science Foundation (SNF) is gratefully acknowledged. A.L. thanks the European Molecular Biology Organization (EMBO) for a long-term fellowship, and H.V.M. acknowledges a stipend by the European Union (Marie Curie).

Keywords: amyloid fibrils · molecular dynamics · prions · solid-state structures

[1] S. B. Prusiner, *Science* **1982**, *216*, 136–144.
[2] G. A. H. Wells, A. C. Scott, C. T. Johnson, R. F. Gunning, R. D. Hancock, M. Jeffrey, M. Dawson, R. Bradley, *Vet. Rec.* **1987**, *121*, 419–420.
[3] R. G. Will, J. W. Ironside, M. Zeidler, S. N. Cousens, K. Estibeiro, A. Alperovitch, S. Poser, M. Pocchiari, A. Hofman, P. G. Smith, *Lancet* **1996**, *347*, 921–925.
[4] A. Lange, B. Meier, *Comptes Rendus Chimie.* **2008**, *11*, 332–339.
[5] S. J. Saupe, *Microbiol. Mol. Biol. Rev.* **2000**, *64*, 489–502.
[6] A. Balguerie, S. Dos Reis, C. Ritter, S. Chaignepain, B. Coulary-Salin, V. Forge, K. Bathany, I. Lascu, J. M. Schmitter, R. Riek, S. J. Saupe, *EMBO J.* **2003**, *22*, 2071–2081.
[7] C. Ritter, M. L. Maddelein, A. B. Siemer, T. Lührs, M. Ernst, B. H. Meier, S. J. Saupe, R. Riek, *Nature* **2005**, *435*, 844–848.
[8] C. Wasmer, A. Lange, H. Van Melckebeke, A. B. Siemer, R. Riek, B. H. Meier, *Science* **2008**, *319*, 1523–1526.
[9] F. Castellani, B. van Rossum, A. Diehl, M. Schubert, K. Rehbein, H. Oschkinat, *Nature* **2002**, *420*, 98–102.
[10] A. Lange, S. Becker, K. Seidel, K. Giller, O. Pongs, M. Baldus, *Angew. Chem.* **2005**, *117*, 2125–2129; *Angew. Chem. Int. Ed.* **2005**, *44*, 2089–2092.
[11] A. B. Siemer, C. Ritter, M. Ernst, R. Riek, B. H. Meier, *Angew. Chem.* **2005**, *117*, 2494–2497; *Angew. Chem. Int. Ed.* **2005**, *44*, 2441–2444.
[12] A. B. Siemer, A. A. Arnold, C. Ritter, T. Westfeld, M. Ernst, R. Riek, B. H. Meier, *J. Am. Chem. Soc.* **2006**, *128*, 13224–13228.
[13] O. C. Andronesi, M. von Bergen, J. Biernat, K. Seidel, C. Griesinger, E. Mandelkow, M. Baldus, *J. Am. Chem. Soc.* **2008**, *130*, 5922–5928.
[14] H. Heise, W. Hoyer, S. Becker, O. C. Andronesi, D. Riedel, M. Baldus, *Proc. Natl. Acad. Sci. USA* **2005**, *102*, 15871–15876.
[15] J. J. Helmus, K. Surewicz, P. S. Nadaud, W. K. Surewicz, C. P. Jaroniec, *Proc. Natl. Acad. Sci. USA* **2008**, *105*, 6284–6289.
[16] W. F. van Gunsteren, D. Bakowies, R. Baron, I. Chandrasekhar, M. Christen, X. Daura, P. Gee, D. P. Geerke, A. Glättli, P. H. Hünenberger, M. A. Kastenholz, C. Oostenbrink, M. Schenk, D. Trzesniak, N. F. A. van der Vegt, H. B. Yu, *Angew. Chem.* **2006**, *118*, 4168–4198; *Angew. Chem. Int. Ed.* **2006**, *45*, 4064–4092.
[17] N. V. Buchete, R. Tycko, G. Hummer, *J. Mol. Biol.* **2005**, *353*, 804–821.
[18] M. Cecchini, R. Curcio, M. Pappalardo, R. Melki, A. Caflisch, *J. Mol. Biol.* **2006**, *357*, 1306–1321.
[19] A. Huet, P. Derreumaux, *Biophys. J.* **2006**, *91*, 3829–3840.
[20] B. Y. Ma, R. Nussinov, *Curr. Opin. Chem. Biol.* **2006**, *10*, 445–452.
[21] B. Tarus, J. E. Straub, D. Thirumalai, *J. Am. Chem. Soc.* **2006**, *128*, 16159–16168.
[22] L. D. Schuler, X. Daura, W. F. van Gunsteren, *J. Comput. Chem.* **2001**, *22*, 1205–1218.
[23] O. C. Andronesi, S. Becker, K. Seidel, H. Heise, H. S. Young, M. Baldus, *J. Am. Chem. Soc.* **2005**, *127*, 12965–12974.
[24] E. R. Henry, A. Szabo, *J. Chem. Phys.* **1985**, *82*, 4753–4761.
[25] J. L. Lorieau, A. E. McDermott, *J. Am. Chem. Soc.* **2006**, *128*, 11505–11512.
[26] K. Seidel, M. Etzkorn, L. Sonnenberg, C. Griesinger, A. Sebald, M. Baldus, *J. Phys. Chem. A* **2005**, *109*, 2436–2442.
[27] A. J. Nederveen, A. Bonvin, *J. Chem. Theory Comput.* **2005**, *1*, 363–374.
[28] P. I. W. de Bakker, P. H. Hünenberger, J. A. McCammon, *J. Mol. Biol.* **1999**, *285*, 1811–1830.
[29] J. H. Missimer, M. O. Steinmetz, R. Baron, F. K. Winkler, R. A. Kammerer, X. Daura, W. F. van Gunsteren, *Protein Sci.* **2007**, *16*, 1349–1359.
[30] M. Sackewitz, H. A. Scheidt, G. Lodderstedt, A. Schierhorn, E. Schwarz, D. Huster, *J. Am. Chem. Soc.* **2008**, *130*, 7172–7173.
[31] A. Karshikoff, R. Ladenstein, *Trends Biochem. Sci.* **2001**, *26*, 550–556.
[32] S. Kumar, R. Nussinov, *Cell. Mol. Life Sci.* **2001**, *58*, 1216–1233.
[33] A. B. Siemer, C. Ritter, M. O. Steinmetz, M. Ernst, R. Riek, B. H. Meier, *J. Biomol. NMR* **2006**, *34*, 75–87.
[34] M. Baldus, A. T. Petkova, J. Herzfeld, R. G. Griffin, *Mol. Phys.* **1998**, *95*, 1197–1207.
[35] B. M. Fung, A. K. Khitrin, K. Ermolaev, *J. Magn. Reson.* **2000**, *142*, 97–101.

[36] B. Elena, A. Lesage, S. Steuernagel, A. Bockmann, L. Emsley, *J. Am. Chem. Soc.* **2005**, *127*, 17296–17302.
[37] G. A. Morris, R. Freeman, *J. Am. Chem. Soc.* **1979**, *101*, 760–762.
[38] E. H. Hardy, R. Verel, B. H. Meier, *J. Magn. Reson.* **2001**, *148*, 459–464.
[39] J. L. Markley, A. Bax, Y. Arata, C. W. Hilbers, R. Kaptein, B. D. Sykes, P. E. Wright, K. Wüthrich, *J. Biomol. NMR* **1998**, *12*, 1–23.
[40] M. Christen, P. H. Hünenberger, D. Bakowies, R. Baron, R. Bürgi, D. P. Geerke, T. N. Heinz, M. A. Kastenholz, V. Kräutler, C. Oostenbrink, C. Peter, D. Trzesniak, W. F. van Gunsteren, *J. Comput. Chem.* **2005**, *26*, 1719–1751.
[41] H. J. C. Berendsen, J. P. M. Postma, W. F. van Gunsteren, J. Hermans in *Interaction Models for Water in Relation to Protein Hydration* (Ed.: B. Pullman), Reidel, Dordrecht, **1981**, pp. 331–342.
[42] H. J. C. Berendsen, J. P. M. Postma, W. F. van Gunsteren, A. Dinola, J. R. Haak, *J. Chem. Phys.* **1984**, *81*, 3684–3690.
[43] J. P. Ryckaert, G. Ciccotti, H. J. C. Berendsen, *J. Comput. Phys.* **1977**, *23*, 327–341.
[44] I. G. Tironi, R. Sperb, P. E. Smith, W. F. van Gunsteren, *J. Chem. Phys.* **1995**, *102*, 5451–5459.

Received: January 10, 2009
Published online on June 5, 2009

